Dynamics and Energy Contributions for Transport of Unfolded Pertactin through a Protein Nanopore

Benjamin Cressiot,[†] Esther Braselmann,[†,¶] Abdelghani Oukhaled,[‡] Adrian H. Elcock,[§] Juan Pelta,[∥] and Patricia L. Clark*[,†,⊥]

[†]Department of Chemistry & Biochemistry, University of Notre Dame, Notre Dame, Indiana 46556, United States, [‡]LAMBE UMR 8587 CNRS, University of Cergy-Pontoise, Cergy-Pontoise, France, [§]Department of Biochemistry, University of Iowa, Iowa City, Iowa 52242, United States, [∥]LAMBE UMR 8587 CNRS, University of Évry-Val-d'Essonne, Évry, France, and [⊥]Department of Chemical & Biomolecular Engineering, University of Notre Dame, Notre Dame, Indiana 46556, United States. [¶]Present address: Department of Chemistry and Biochemistry, BioFrontiers Institute, University of Colorado, Boulder, CO 80303.

ABSTRACT To evaluate the physical parameters governing translocation of an unfolded protein across a lipid bilayer, we studied protein transport through aerolysin, a passive protein channel, at the single-molecule level. The protein model used was the passenger domain of pertactin, an autotransporter virulence protein. Transport of pertactin through the aerolysin nanopore was detected as transient partial current blockades as the unfolded protein partially occluded the aerolysin channel. We compared the dynamics of entry and transport for unfolded pertactin and a covalent end-to-end dimer of the same protein. For both the monomer and the dimer, the event frequency of current blockades increased exponentially with the applied voltage, while the duration of each event decreased exponentially as a function of the electrical potential. The blockade time was twice as long for the dimer as for the monomer. The calculated activation free energy includes a main enthalpic component that we attribute to electrostatic interactions between pertactin and the aerolysin nanopore (despite the low Debye length), plus an entropic component due to confinement of the unfolded chain within the narrow pore. Comparing our experimental results to previous studies and theory suggests that unfolded proteins cross the membrane by passing through the nanopore in a somewhat compact conformation according to the "blob" model of Daoud and de Gennes.

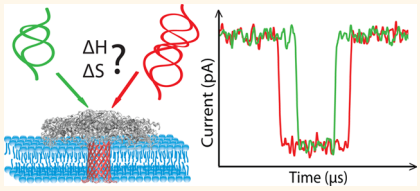

KEYWORDS: protein nanopore · electrical detection · autotransporters · secretion · single molecule · translocation · unfolded protein

Every cell is defined by a lipid membrane boundary. Within this membrane, protein channels are used to transport proteins and other molecules to the cell surface, where they enable the cell to sense and interact with its environment. Protein transport across a membrane, known as translocation, is a decisive step in the biosynthesis of many proteins as it aids in proper folding and thus biomolecular function.[1,2] One-half of the eukaryotic proteome is translocated across a membrane in an unfolded state prior to reaching its final, functional destination,[1,2] and hence it is of vital importance to understand these translocation mechanisms and their connection to protein folding and function. Typically, the energy required to translocate a protein through a nanometer-scale protein channel is provided by a motor powered by ATP (or GTP) hydrolysis,[3,4] a Brownian ratchet,[5] or entropic pulling.[6]

To enable a more detailed analysis of the physical forces underlying protein translocation, we used a single-molecule nanopore assay to study the transport of an unfolded protein through a protein channel embedded within a lipid membrane. Using this approach, it has been possible to describe the transport and structure of peptides,[7−11] protein transport dynamics through toxins[7,12,13] and mitochondrial channels,[4,14] and protein−pore[15,16] and protein−protein interactions.[17] Protein nanopores have also emerged as powerful tools to study protein unfolding transitions using chemical denaturing agents,[18,19] thermal denaturation,[20] or an electric field[21,22] at the single-molecule level. Recently, Akeson's group used the energy of ATP hydrolysis provided by the AAA+ unfoldase ClpX to transport folded proteins through α-hemolysin.[23,24] Protein nanopores have also been used to study protein folding with cationic ions[25,26] and detect protein phosphorylation.[27]

We used aerolysin, a well-characterized passive protein-forming channel from

* Address correspondence to pclark1@nd.edu.

Received for review May 25, 2015 and accepted August 21, 2015.

Published online August 24, 2015
10.1021/acsnano.5b03053

Aeromonas hydrophila. Aerolysin has an inner pore diameter of 1.0−1.7 nm,[12,28,29] similar to the dimensions of the translocation channel within many other transmembrane proteins, including autotransporter translocator domains[30−36] and members of the BamA family.[37,38] As with these other protein channels,[39−41] aerolysin is known to translocate only non-native proteins.[12,19,20,42] Aerolysin has been used for numerous single-molecule studies of protein and peptide translocation.[7,12,19,20,42] For transport of completely unfolded maltose binding protein (MBP) through aerolysin, increasing the applied voltage resulted in an increase of the event frequency and a decrease in the time of translocation.[12,18] Furthermore, aerolysin has been used to study unfolding of proteins at the single-molecule level,[19,20] including the detection of partially unfolded states.[19] Collectively, aerolysin and α-hemolysin have been used extensively to characterize the transport of completely unfolded and partially folded proteins through a protein channel (reviewed in refs 43 and 44), providing an opportunity to compare translocation of our model protein to the translocation mechanism for other unfolded proteins.

In this study, we investigated transport of the passenger domain of pertactin, an autotransporter virulence protein from *Bordetella pertussis*, through a single aerolysin nanopore. Autotransporter proteins are a large and diverse class of monomeric virulence proteins secreted from Gram-negative bacterial pathogens.[45] The translocation of the autotransporter passenger domain, which represents the mature virulence protein, across the bacterial outer membrane is mediated by its own cotranslated C-terminal transmembrane translocator domain and the folding properties of the passenger.[40,41,46] Pertactin is an extracellular integrin binding protein that mediates attachment of *B. pertussis* to the ciliated cells of the upper respiratory system.[47] The pertactin passenger domain is 539 aa long and has a predicted net charge of −2.4*e* at pH 7.5. Its β-helical native structure is roughly cylindrical, with a length of 10 nm and diameter of 4 nm.[48]

Here we characterized the translocation of unfolded pertactin passenger through the well-characterized aerolysin nanopore using an applied potential in order to study the fundamental physical parameters that govern translocation of an unfolded protein through a narrow pore within a membrane. Specifically, we determined experimentally the contributions of entropy and enthalpy to pertactin translocation and compared these results to previous studies of the translocation properties of unfolded MBP through aerolysin[12] in order to determine to what extent translocation is affected by protein length and net charge. Surprisingly, our results revealed that unfolded pertactin dynamics through aerolysin exhibit the same dependence on applied voltage as MBP, despite significant differences in protein length and net charge.[12] These results suggest that translocation of an unfolded protein is dominated by an activation energy that has an enthalpic origin, mainly arising from interactions between the chain and the pore. In addition, there is an entropic component due to the confinement of the polypeptide chain at the entry of the pore.

RESULTS AND DISCUSSION

Principle of the Experiment. The nanopore experimental setup consisted of a single aerolysin nanopore inserted into a lipid membrane, connecting two compartments filled with an electrolyte solution. A Ag/AgCl electrode was inserted into each compartment and used to generate an ionic current through the pore (Figure 1a,b). This current provided the driving force to transport the negatively net charged unfolded pertactin passenger through the nanopore, which resulted in a brief partial current blockade. In the absence of pertactin, the ionic current of the empty pore remained constant (Figure 2a), confirming that detected events occur solely due to pertactin rather than from instability of the pore.

Because the aerolysin nanopore is stable only up to 1.5 M GdnHCl,[12] we studied the translocation of a destabilized pertactin passenger variant, pertactin-2K (see Methods). Pertactin-2K has seven tryptophan residues distributed throughout its sequence; hence changes in tryptophan fluorescence emission reflect the global unfolding of the protein. Pertactin-2K was completely unfolded in 1 M GdnHCl, as determined from ensemble measurements of tryptophan fluorescence emission as a function of denaturant concentration (Supporting Information Figure S1a). Although less stable than the wild-type pertactin passenger, pertactin-2K is efficiently secreted *in vivo* (Supporting Information Figure S1b) and is hereafter referred to as pertactin. When unfolded pertactin in 1 M GdnHCl was added to each compartment, current blockades were detected (Figure 2). Note that in 1 M GdnHCl aerolysin remains stably folded in the lipid membrane.[12]

In the presence of pertactin, we observed two kinds of current blockades associated with two types of events: (*i*) "bumping" events (not shown), characterized by brief, low-level current blockades, which arise due to diffusion of pertactin close to the pore; and (*ii*) translocation events, characterized by larger current blockades of longer duration (Figure 1b). These two types of events are typically seen during nanopore translocation of DNA,[49−51] polyelectrolytes,[52−54] and unfolded proteins.[12,18,19] In order to characterize the transport dynamics of pertactin into aerolysin, each current trace was statistically analyzed to determine the frequency of blockade events, blockade duration, and level of current drop and to separate bumping events from translocation events (see Methods).

Effect of Pertactin Concentration. Increasing the pertactin concentration resulted in a corresponding linear increase

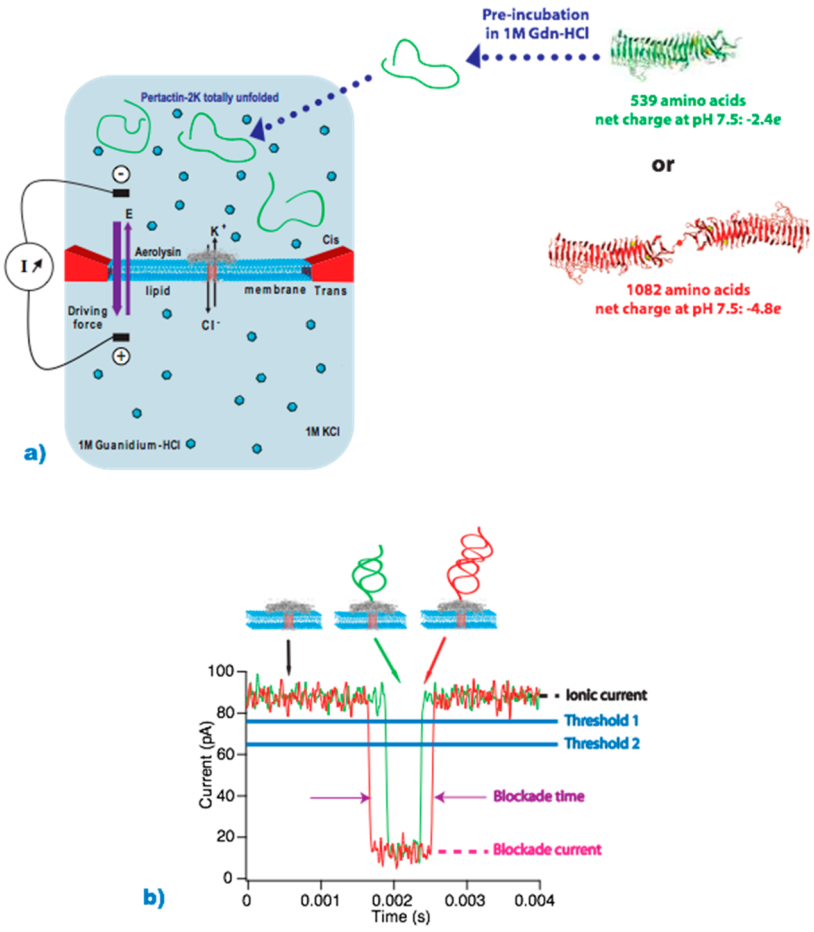

Figure 1. Principle of protein detection using an aerolysin pore inserted into a lipid membrane. One aerolysin nanopore is inserted in a suspended lipid bilayer (a). An electrical potential is applied, which induces a current in the nanopore due to the presence of K^+ and Cl^- ions in the bulk solution and their transport through the nanopore. Unfolded pertactin or the covalent dimer was added to both compartments. Both pertactin and the dimer are negatively charged under our conditions, with a net charge of $-2.4e$ and $-4.8e$, respectively. The aerolysin ribbon diagram shown here and in all other figures was adapted from ref 28 with permission. (b) Single-channel current trace for transport of unfolded pertactin (green) or unfolded dimer (red) through an aerolysin pore at 100 mV. Indicated are the ionic current of an empty pore (I_0), blockade current (I_B), blockade duration (τ_t), and the thresholds used to distinguish translocation events from bumping and noise (see Methods). Unfolded pertactin enters by the *cis* side of the aerolysin. Experiments are performed in 1 M KCl, 25 mM HEPES, pH 7.5, with 1 M GdnHCl as the denaturing agent.

of the frequency of translocation events (long-duration current blockades) (Figure 2). However, the duration of each event was concentration-independent (Figure 2f), with a mean blockade time of 664 ± 24 μs (standard deviation; SD) at 70 mV (from seven separate pores, with an average of 752 individual events measured per pore). To test whether there were attractive interactions between pertactin and the entrance to the nanopore, we calculated the rate constants for dissociation (k_{off}) and association (k_{on}) and used these to calculate the dissociation constant (K_d). The k_{off} and k_{on} are related to measurable features of the binding events *via* $k_{off} = 1/\tau_t$ and $k_{on} = 1/(c\tau_i)$, with c representing the concentration of protein, and τ_i and τ_t are the mean interevent time and blockade time, respectively.[43] We found $k_{off} = 1.54 \times 10^3 \pm 0.21 \times 10^3\ s^{-1}$ and $k_{on} = (6.80 \pm 4) \times 10^{-2}\ M^{-1}\ s^{-1}$. These rate constants yield a dissociation constant, $K_d = k_{off}/k_{on}$, of $2.26 \times 10^2 \pm 0.31 \times 10^2$ M. The standard free energy, $\Delta G^0 = -RT \ln(1/K_a)$, is therefore $\Delta G^0 = 13.4 \pm 0.1$ kJ mol^{-1} at 70 mV. Consistent with previous studies,[12,43] the linear correlation between event frequency and protein concentration, along with the independence of blockade time to protein concentration and high calculated K_d, demonstrate that pertactin−aerolysin interactions represent a reversible bimolecular reaction, with no strong attractive interaction at the entrance of the pore.

Translocation of Unfolded Pertactin Is Well-Described by an Activation Barrier Model. To measure the energy barrier for entry of pertactin into the nanopore, we varied the electric field. Adjusting the applied voltage between 35 and 110 mV resulted in an increase of the ionic current of the empty pore and in the frequency of current blockades due to pertactin translocation (Figure 3a−c). The interevent time distribution was well fit by a single exponential equation (Figure 4a). It has previously been shown that entry of an unfolded protein into a nanopore follows the van't Hoff−Arrhenius relationship[7,12]

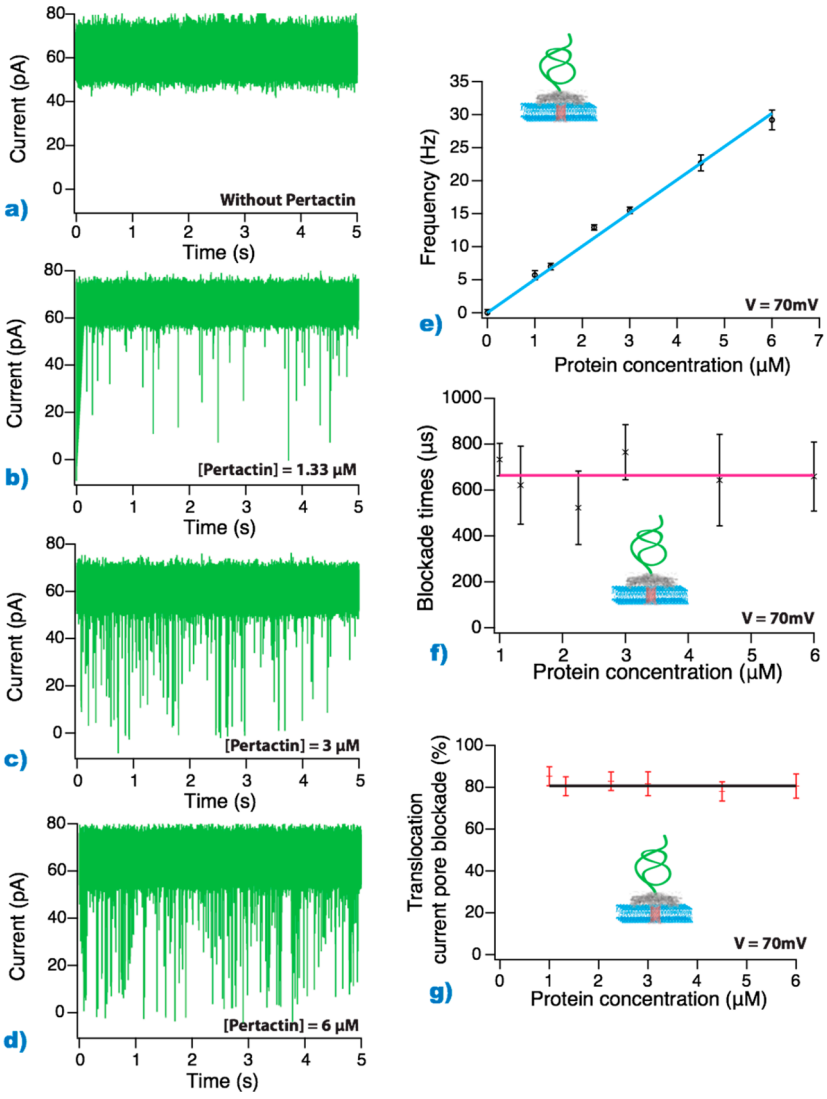

Figure 2. Transport dynamics of unfolded pertactin as a function of protein concentration through a single aerolysin pore. Detail of current traces recorded through an aerolysin channel in the absence or presence of unfolded pertactin at different protein concentrations: (a) 0 μM, (b) 1.3 μM, (c) 2.0 μM, or (d) 6.0 μM pertactin. An increase of the protein concentration results in an increase of blockade events frequency. (e) Frequency of events as a function of the protein concentration at an applied potential of 70 mV. The blue line is a linear fit; slope = 4.84 $\pm$ 0.16 Hz M^{-1} (SD). (f) Blockade time of unfolded pertactin as a function of the protein concentration. The applied voltage is 70 mV. The mean blockade time is 664 $\pm$ 24 μs (pink line). (g) Translocation current pore blockade $\{[1 - (\langle I_B \rangle / \langle I_0 \rangle)] \times 100\}$ as a function of the protein concentration. The mean current pore blockade is 80 $\pm$ 10% (black line). The experiments are performed in 1 M KCl, 25 mM HEPES, pH 7.5, with a final guanidinium concentration of 1 M.

$f = f_0 \exp(V/V_0)$ (Figure 4b), where $f_0 = p \exp(-U^*/k_BT)$ is the translocation event frequency in the absence of applied voltage, p is a frequency factor (defined by $p = cDA/L$, where c is the bulk concentration of the protein, D is its translational diffusion coefficient (see below), A is the cross-sectional area of the channel, and L is the pore length), U^* is the activation free energy, k_B is the Boltzmann constant, T is the temperature, and $V_0 = k_BT/ze$, where z is defined as the effective charge of the protein on which the electric field acts at the pore entrance and e is the elementary charge of an electron. We found $f_0 = 1.0 \pm 0.1$ Hz, $V_0 = 39.0 \pm 0.3$ mV, and $z = 0.66 \pm 0.10$ at the pore entrance (Figure 4b).

To further investigate the underlying thermodynamics of pertactin translocation through the nanopore, we constructed a covalent pertactin dimer. The dimer consists of two copies of pertactin bearing an alanine–cysteine motif at the C-terminus, connected *via* a disulfide bond (Figure 1a). The average translocation blockade time for this covalent dimer was approximately twice as long as events recorded for the monomer (Figures 1b and 4d). These results are consistent with translocation of a chain twice as long and, taken together with the decrease in blockade time with increasing applied potential (Figure 4d), indirectly demonstrate that the long and deep current blockade events corresponded to protein translocation, rather

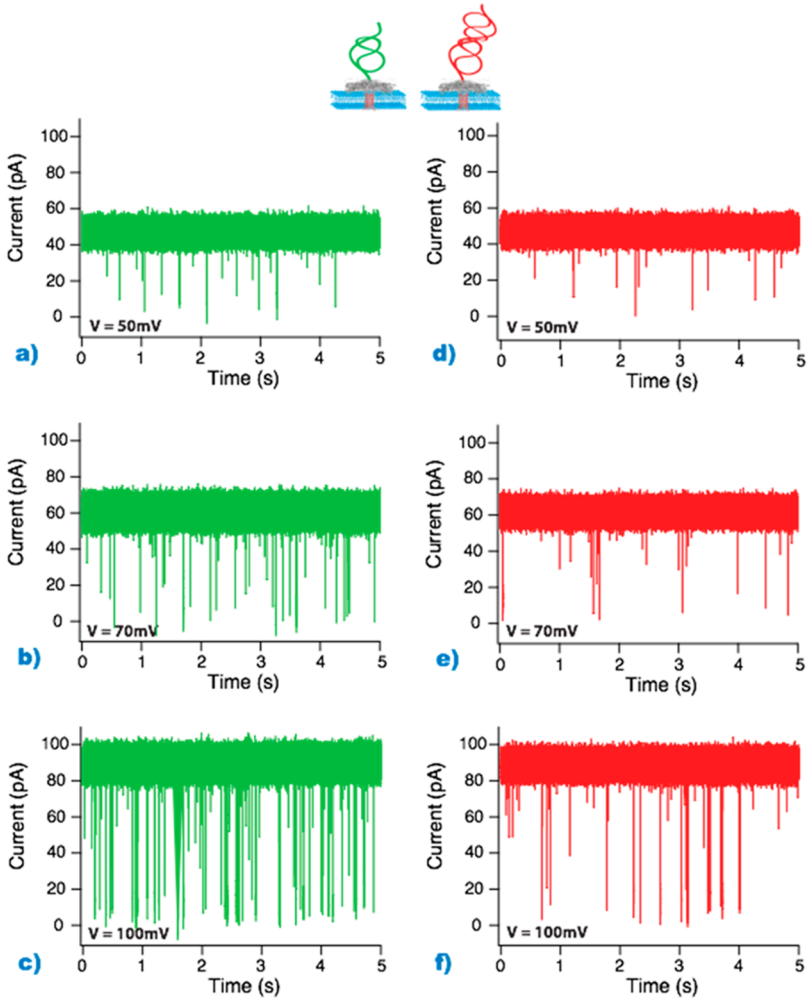

Figure 3. Detail of current traces recorded though a single aerolysin pore for different applied voltages. Concentration of pertactin was 1 μM. Current traces were measured at (a) 50 mV, (b) 70 mV, or (c) 100 mV or in the presence of the pertactin dimer at (d) 50 mV, (e) 70 mV, or (f) 100 mV. Increasing the applied voltage resulted in an increase of the open pore current and the frequency of blockade events for each protein.

than unproductive "bumping" collisions between pertactin and the nanopore. Applying the same van't Hoff–Arrhenius analysis described above returned values for the dimer nearly identical to the monomer ($f_0 = 0.95 \pm 0.09$ Hz, $V_0 = 41.0 \pm 0.2$ mV, and $z = 0.63 \pm 0.08$ at the pore entrance). Note that the exponential dependence of the event frequency as a function of the applied voltage observed for both pertactin and the dimer also describes the transport of other unfolded proteins,[12,18] peptides,[7,13] and DNA[49−51] and polyelectrolytes[52−54] through α-hemolysin and aerolysin.

To calculate the energy barrier for entry of pertactin inside the aerolysin, we first calculated the expected translational diffusion coefficients for pertactin and the dimer using HYDROPRO,[55] which returned mean values of $D = 2.81 \times 10^{-11}$ m^2 s^{-1} for pertactin and 1.98×10^{-11} m^2 s^{-1} for the dimer (see Methods for a complete description). For a protein concentration of 1 μM (6×10^{20} molecules m^{-3}), a cylindrical pore with a diameter of 1.7 nm (only the larger diameter of the pore will be used), and a length of 10 nm, we obtained $p = 14.7$ s^{-1} for pertactin and $p = 10.7$ s^{-1} for the dimer. Using $f_0 = p \exp(-U^*/k_BT)$ and the values of f_0 determined above, the energy barrier for entry of both pertactin and the covalent dimer inside the aerolysin was calculated as $U^* \cong 2.5 \pm 0.2\ k_BT$. This result was initially surprising: given that the bulk diffusion rate is slower for the dimer than the monomer, we expected an increase of the free energy barrier for its entry into the nanopore. However, this may be compensated by the higher probability for the dimer to populate the capture zone, which is on the micrometer scale.[56]

Pertactin and the dimer had the same energy barrier for entry into the channel, indicating that protein–nanopore interactions initiated protein transport through the channel, as previously observed for other protein transport systems.[12,19,42,52,57−59] Hence, at low potentials, we expect the blockade time to decrease exponentially with the applied voltage.[12,52,60] For both pertactin and the dimer, the mean blockade duration was best fit to an exponential function $y = B \exp(-V/V_c)$, with B representing the duration of the

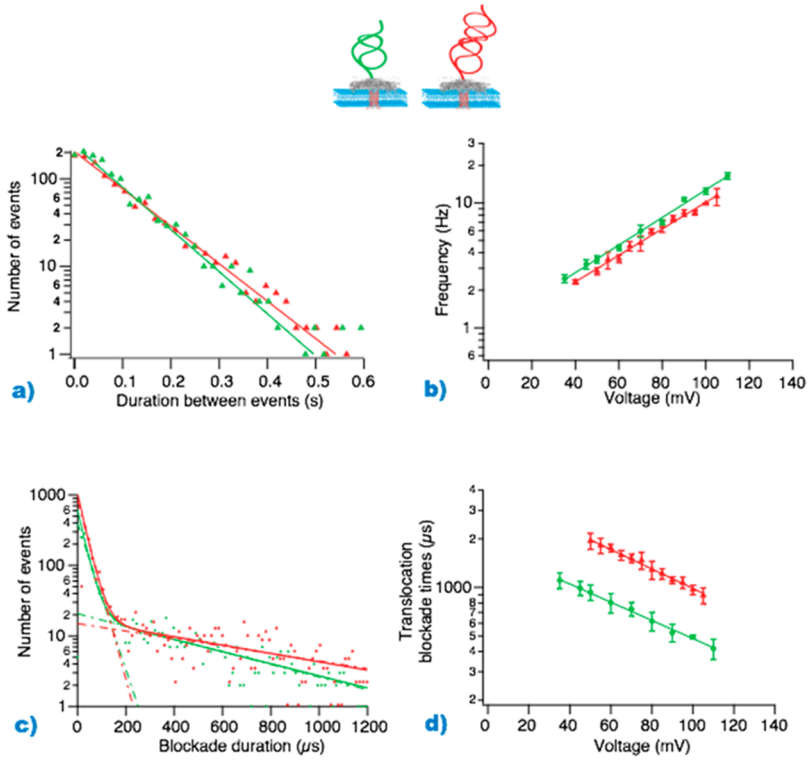

Figure 4. Frequency and duration of unfolded pertactin and unfolded dimer transport events as a function of the applied voltage. (a) Distribution of duration between events for unfolded pertactin (green) and unfolded dimer (red) at 100 mV. Lines correspond to exponential fits. (b) Frequency of events as a function of the applied voltage. The green and red lines are exponential fits to the equation $f = f_0 \exp(V/V_0)$; see main text for a complete description. (c) Distribution of blockade duration for unfolded pertactin (green) or unfolded dimer (red); dotted lines are single exponential fits, and solid lines are double exponential fits. (d) Current pore blockade times for translocation events as a function of the applied voltage: $f(V) = B \exp(-V/V_c)$, where B is the long blockade duration in the absence of applied voltage. We found for pertactin, $B = 1761 \pm 65$ μs (SD) and $V_c = 77 \pm 1$ mV (SD), and for the dimer, $B = 3946 \pm 91$ μs (SD) and $V_c = 72 \pm 2$ mV (SD). Experiments were performed in 1 M KCl, 25 mM HEPES, pH 7.5, with 1 M GdnHCl.

transport event in the absence of an applied voltage and V_c the electric field acting on the protein effective charge at the pore entrance (Figure 4d and Supporting Information Figure S1c,d). For pertactin, the exponential fit returned $B = 1761 \pm 65$ μs and $V_c = 77 \pm 1$ mV, and for the dimer, $B = 3946 \pm 91$ μs and $V_c = 72 \pm 2$ mV. Hence, under our experimental conditions, an energy barrier due to protein−channel interactions governs transport of unfolded proteins.

We also considered whether electro-osmotic flux could provide the main driving force for transport of unfolded pertactin through the nanopore. It is well-established for nanopore translocation of natural and synthetic polyelectrolytes and proteins that when an electrical potential is the dominant driving force, the event frequency increases exponentially with the applied voltage (V) while average blockade time decreases.[12,52,60] If electro-osmotic flux was instead the dominant driving force for the transport of macromolecules through the nanopore, we would expect a linear increase of frequency and blockade times as a function of the applied voltage. In our study, we found an exponential dependency for both event frequency and blockade time (Figure 4b,d), demonstrating that transport of unfolded pertactin was governed by the electric driving force and not by electro-osmotic flux.

Interestingly, for a narrow (3 nm) solid-state nanopore, the blockade time for an unfolded protein also decreased exponentially at similar voltages (200−400 mV).[61] In contrast, the blockade time was inversely proportional to voltage at much higher potentials (400−750 mV). These results are consistent with a model in which at low−medium potentials the confinement of the protein in the pore creates an entropic barrier to transport, yet at higher potentials, transport is enabled *via* an electrophoretic mechanism. In our experimental setup, the largest potential used was 110 mV because, above 110 mV, the diameter of the aerolysin pore becomes voltage-sensitive.[62] Thus, this setup is not conducive to detecting an electrophoretic transport mechanism at higher applied potentials, and pertactin translocation for all experimental conditions in our study can be described by an energy barrier model.

Entry of Unfolded Proteins Is Mainly Controlled by Enthalpy Rather than Entropy. Having determined that under our conditions an activation barrier governed pertactin transport, we next calculated the relative contributions of enthalpy and entropy to this barrier. The end-to-end distance of pertactin and the dimer were estimated

using $R \approx aN^{\nu}$, with a representing the average monomer size in the longitudinal and transverse directions with respect to the persistence length (a = 0.66 ± 0.05 nm),[63] N the numbers of monomers at this persistence length (given that a persistence length of 0.66 nm corresponds to the diameter of two amino acids, N = 539/2 = 270), and ν the Flory exponent describing chain conformation.[64] Typically, ν = 1/2 is used for a random coil chain in an ideal solvent or ν = 3/5 for an expanded chain in a "good" solvent. We found R = 11 or 19 nm for pertactin and 16 or 29 nm for the covalent dimer, respectively, for ν = 1/2 or ν = 3/5. We can also evaluate the radius of gyration (R_g) from the diffusion coefficient: the hydrodynamic radius is defined as $R_H = k_BT/(\eta 6\pi D)$, with the viscosity of water $\eta = 8.91 \times 10^{-4}$ kg m^{-1} s^{-1}, and R_H/R_g = 0.8 for an ideal chain or 0.64 for an excluded volume chain.[64] We found R_H = 9.7 nm for the monomer and 12.4 nm for the covalent dimer and R_g = 10.9 or 13.6 nm for the monomer and 15.4 or 19.3 nm for the covalent dimer. In all cases, these estimated protein dimensions are much larger than the dimensions of the aerolysin nanopore (maximum diameter 1.7 nm).[28,29] The activation free energy estimated for the entry of pertactin into the aerolysin thus necessarily includes an entropic contribution due to the confinement of the chain at the pore entrance.[65,66] Yet if the origin of the energy barrier for entry of pertactin into the nanopore was purely entropic, we would expect a larger activation barrier for the covalent dimer due to its larger size.

Previously, we studied transport of unfolded MBP through aerolysin.[12] MBP is significantly shorter than pertactin (370 aa *versus* 539 aa, respectively) and has a different net charge (−8*e* *versus* −2.4*e*, respectively). If transport of an unfolded protein through a nanopore was governed by the loss of entropy that occurs upon confinement of the entire chain within the channel, the translocation blockade time for pertactin should be longer than for MBP under identical conditions,[12] reflecting the longer chain length of pertactin. Yet surprisingly, the mean blockade duration measured for pertactin through aerolysin (τ_t = 733 ± 71 μs at 70 mV) is indistinguishable from that measured previously for MBP (τ_t = 732 ± 31 μs at 70 mV), indicating that, as for chain entry into the nanopore, entropy alone also does not govern transport through the nanopore.

To determine why two proteins of different sizes have indistinguishable blockade durations, we first compared our results with published results on the transport of unfolded MBP through the same pore under identical conditions,[12] Pastoriza-Gallego *et al.* calculated an energy barrier for MBP as U^* = 4 k_BT. The radius of unfolded MBP was estimated from 6 nm (ν = 1/2; ideal random coil chain) to 12 nm (ν = 3/5; expanded chain). The theoretical free energy for confinement of a neutral polymer is estimated by the relation $U^* \cong k_BT(R/d)^{1/\nu} \cong k_BTN \times (a/d)^2$, where N is the number of amino acids, a the size of an amino acid, and d the nanopore diameter.[67] With a purely entropic barrier, we expect $U^*_{pertactin} = U^*_{MBP} \times (N_{pertactin}/N_{MBP}) = U^*_{MBP} \times 1.45$ = 5.8 k_BT for pertactin and 11.7 k_BT for the covalent dimer. Yet we observed instead a decrease of the activation barrier for transport of both pertactin and its dimer (2.5 k_BT) relative to MBP (4 k_BT). This result is consistent with the results above for translocation of the pertactin monomer *versus* dimer, confirming that entry of pertactin into the nanopore is not governed solely by entropy.

Having established that the energy barrier for pertactin translocation has enthalpic as well as entropic components, we next compared our results to those for the entry of highly charged macromolecules into a narrow pore. Our measured value of the activation barrier for pertactin, $U^* \cong$ 2.5 k_BT, is lower than values found for highly charged macromolecules at high ionic strength through α-hemolysin (for DNA,[49,50] $U^* \cong$ 8 k_BT, while for dextran sulfate,[52] $U^* \cong$ 10 k_BT). At 1 M KCl, the Debye length in our experiments is 0.3 nm, lower than the Bjerrum length (0.7 nm), which is the length where electrostatic interactions are the order of the thermal agitation.[68] Although electrostatic interactions will be screened by the salt ions, electrostatic interactions could nevertheless contribute an enthalpic component[69] to pertactin entry into the aerolysin nanopore. Note, in particular, that both pertactin and the dimer have a negative net charge (−2.4*e* and −4.8*e*, respectively). In contrast, aerolysin has 91 charged residues, with an overall net charge of +7*e* in the channel.[28] The difference observed in the activation barrier between the pertactin constructs and MBP could thus be explained by net charge differences, with the pertactin constructs having less charge per unit length (−1*e*/224 amino acids) than MBP (−1*e*/46 amino acids). Electrostatic interactions with MBP at the entry of the pore could therefore explain its larger activation free energy.

To calculate the precise contributions of enthalpy *versus* entropy to pertactin translocation, we used the experimental free energy change of a single polymer partitioning into a pore.[70,71] Because the covalent dimer is twice the length of pertactin, we were able to extract experimentally the entropic barrier contribution for the entry of the proteins inside the pore:

$$\Delta U_{\text{dimer}\rightarrow\text{monomer}} = k_BT \ln\left(\frac{\Pi_{\text{dimer}}}{\Pi_{\text{monomer}}}\right)$$

The partition coefficient Π reads $\Pi = (1/N_A v_{pore})(Pr)$, where N_A is the Avogadro constant, v_{pore} represents the pore volume, and the residence probability $Pr = \tau_{occup}/(\tau_{tot}c)$, where τ_{occup} is the time occupied per protein inside the pore, τ_{tot} is the total acquisition time, and c is the protein concentration.[72] Thus, $\Delta U_{dimer\rightarrow monomer} = U_{entropic} = k_BT \ln(Pr_{dimer}/Pr_{monomer})$ = 0.73 ± 0.04 k_BT, which is the estimated entropic contribution. The estimated enthalpic contribution therefore

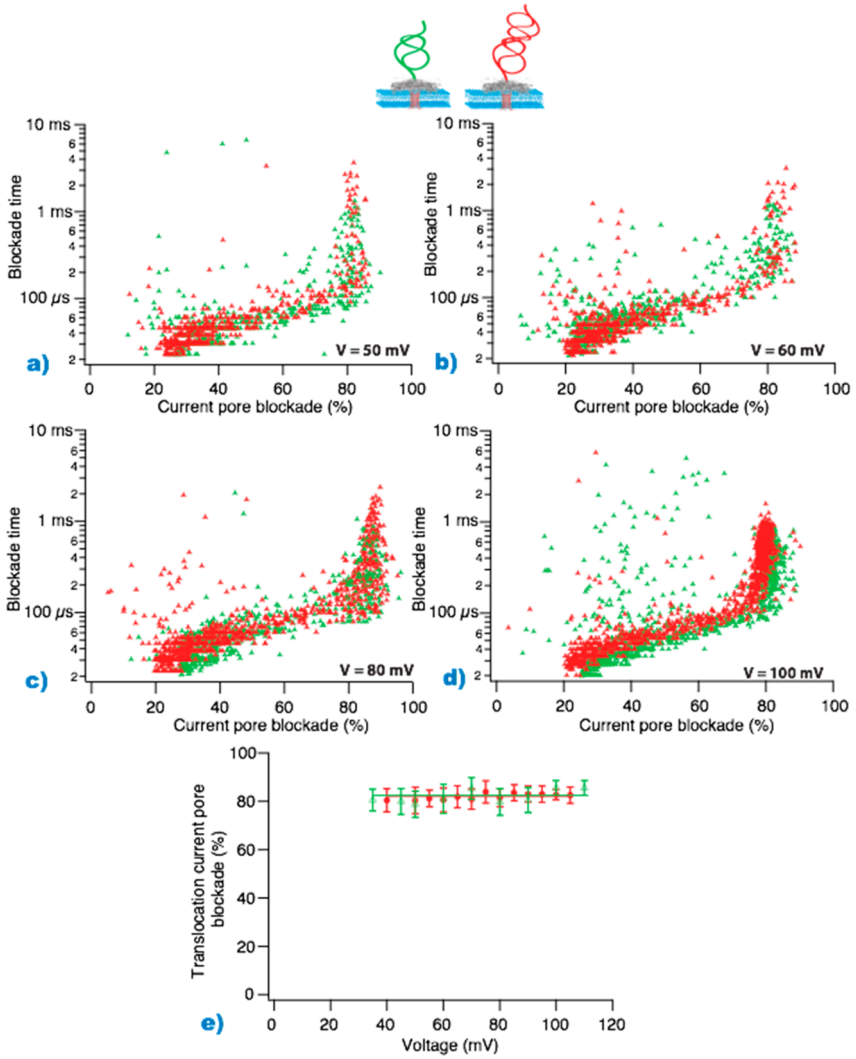

Figure 5. Scatter plot of blockade times *versus* current pore blockade for pertactin (green) and the covalent dimer (red). The applied potential was (a) 50 mV, (b) 60 mV, (c) 80 mV, or (d) 100 mV. (e) Current pore blockade for pertactin (green) and dimer (red) transport events as a function of the applied voltage. The mean current pore blockade is 82 ± 9% for pertactin (green line) and 82 ± 9% for the dimer (red line).

is $U_{enthalpic} = U^* - U_{entropic} \cong 1.8 \pm 0.2\ k_BT$. These results are consistent with those above, where the entry of unfolded pertactin is controlled by enthalpy rather than entropy. Unfortunately, we cannot use this approach to calculate the energy contributions for MBP translocation because the MBP dimer used previously was studied at only one applied voltage.[12]

Pertactin Is Transported Inside the Nanopore in a Blob Conformation. In order to determine the conformation of pertactin during its translocation through aerolysin, we compared the percentage of the electrical current pore blockade for the transport events as a function of voltage (Figure 5a–d) and protein concentration (Figure 2g). The translocation current pore blockade times are independent of the applied voltage (Figure 5e) and the protein concentration (Figure 2g). The current pore blockade was 80 ± 10% when calculated from results at a variety of protein concentration or 82 ± 9% (for both pertactin and the covalent dimer) when calculated from results at different applied voltages.

The current pore blockade is proportional to the volume occupied by the chain inside the pore. The persistence length of an unfolded polypeptide chain in excluded volume conformation (l_p = 6.6 Å)[63] is likely a realistic value for our experimental conditions. If unfolded pertactin or the dimer was fully extended inside the pore, it would occupy a roughly cylindrical volume with $r_{monomer} = 0.33 \pm 0.02$ nm, corresponding to the average radius of two amino acids.[63] The predicted percentage volume occupied by the extended portion of the protein passing through the nanopore is given by the volume of the protein, v_{prot}, divided by the volume of the pore v_{pore}: $v_{prot}/v_{pore} = r_{monomer}^2/r_{pore}^2 = 15 \pm 4\%$ (using a maximal pore radius of 0.85 nm)[28] to 45 ± 12% (using the minimal pore radius of 0.5 nm). Yet the average measured current blockade was much higher (~80%), indicating that pertactin and the dimer

do not adopt a fully extended conformation inside the nanopore. In contrast, unfolded proteins did adopt a fully extended conformation at higher voltages within a narrow solid-state nanopore.[61,73]

We considered whether the higher average measured current blockade could be higher than expected for a fully extended conformation because pertactin enters the pore with its ion cloud (Manning condensation), as has been observed for polyelectrolytes at high salt concentration.[54,74] It is important to note, however, that in pertactin (as for most proteins) there is no significant clustering of positively or negatively charged amino acids. Nevertheless, to test this, we calculated the theoretical linear density of charge,[75] given by $\xi = l_B/b$, where l_B is the Bjerrum length (l_B = 7.14 Å) and b is the average distance between neighboring charged monomers. We expect ion condensation if $\xi > 1/|Z_iZ_n|$, with Z_i and Z_n being the valence of the ion and polyampholyte, respectively. If we take into account the persistence length, l_p, pertactin is 539 aa long (corresponding to 539/2 monomers) and has a predicted net charge of $-2.4e$ at pH 7.5, yielding b = ((539/2)/2.4) × 6.6 = 741 Å between charges (recall that the diameter of one monomer = 6.6 Å). Hence ξ = 7.14/741 = 0.01. This linear density of charge is below 1. According to Manning's theory, most of the ions are thus free rather than condensed along the protein chain.[75] Alternatively, theoretical linear density of charge can be estimated using the average distance between two successive charges in pertactin. The average distance between two charged residues in pertactin is 7, yielding ξ = 7.14/(7 × 6.6) = 0.2, corroborating our conclusion that ions are mainly free in bulk solution.

To further explore the conformation of pertactin within the aerolysin nanopore, we used the model proposed by Daoud and de Gennes,[76] which considers the protein inside the pore as a flexible chain forming a necklace of spherical blobs of diameter d, equivalent to the diameter of the pore, and $d = r_{monomer}g^{3/5}$, where $r_{monomer}$ is the radius of an amino acid and g is the number of amino acids per blob for an excluded volume chain conformation. We found from the previous equation that g = 15 aa per spherical blob. Because the aerolysin channel is 10 nm long, approximately five blobs fit inside the channel, for a total of ~75 pertactin residues within the aerolysin nanopore during its translocation. In comparison, we would expect only 30 residues to reside within the nanopore if the unfolded protein was fully extended.

Interestingly, we estimated the effective charge of pertactin and the dimer inside the aerolysin pore, z_{inside}, from the blockade times as a function of the applied voltage (Figure 4d), defined as $z_{inside} = k_BT/V_ce$. We found z_{inside} = 0.33 ± 0.02 for pertactin and 0.35 ± 0.01 for the dimer. We found the predicted number of amino acids in the aerolysin channel to be 75 for the monomer and 79 for the dimer, as calculated solely from the effective charge on the portion of the protein within the channel (z_{inside}) *versus* overall net charge (−2.4*e* for the monomer or −4.8*e* for the dimer). These results corroborate that both pertactin and the covalent dimer were not stretched by the applied electric field used in our conditions and instead adopt a non-extended conformation during transport through the channel.

CONCLUSIONS

We have shown that an activation barrier model governs the transport of unfolded pertactin through aerolysin as a function of the applied voltage, as shown in previous studies with other peptides and proteins.[7,12] For completely unfolded protein, a van't Hoff−Arrhenius law described the frequency of blockades as a function of the applied voltage for a nanopore with a radius smaller than the macromolecule size. At low applied voltage, the transport times decrease exponentially when increasing the applied voltage. We have determined experimentally, for the first time, the enthalpic and entropic contribution for the entry of an unfolded protein inside a narrow protein nanopore. The activation barrier for entry of unfolded pertactin into aerolysin is mainly controlled by enthalpy rather than entropy. However, we may be at the limit of the model used to extrapolate the energy barrier for the translocation, being entry and transport processes, of proteins into the pore. We demonstrated that at low electrical driving force these unfolded proteins translocated through the aerolysin nanopore in a non-extended conformation, as previously observed for a neutral polymer,[71] according to the Daoud and de Gennes "blob" model.[76]

METHODS

Nanopores. Membrane lipid bilayers were made according to previously described methods[78] In brief, a film of a 1% solution of diphytanoylphosphatidylcholine lecithin (Avanti) in decane was spread across a 150 μm diameter hole drilled in the polysulfone wall separating the two compartments of a chamber. Each compartment contained 1 mL of 1 M KCl, 25 mM HEPES, pH 7.5. After the decane film was thinned and a planar bilayer formed, a single channel was created by adding monomeric recombinant aerolysin from a stock solution in one compartment.

Aerolysin was expressed and purified from *Escherichia coli* BL21(DE3)pLysS as proaerolysin, as described previously,[79] and was activated by digestion with trypsin for 10 min at room temperature to eliminate the pro-peptide sequence, allowing monomers to polymerize.[80]

Proteins. Pertactin-2K is a variant of the wild-type passenger sequence.[77] We introduced two destabilizing mutations in the S298P background (the variant used to crystallize pertactin[48]). The destabilizing mutations I401K and L464K introduce positive charges in the hydrophobic core of the pertactin native structure. Pertactin-2K was purified according to standard procedures

analogous to those for wild-type pertactin.[77] Briefly, the protein is refolded from inclusion bodies by stepwise dilution and dialysis. The refolded protein is purified by ion exchange chromatography and size-exclusion chromatography.

For the pertactin covalent dimer, we introduced alanine and cysteine residues at the C-terminus of pertactin-2K. Covalent disulfide bonded dimers formed spontaneously during purification and were purified as for pertactin-2K.

We used the following equation[81] to calculate net charge:

$$\text{net charge} = \sum_i Ni \frac{10^{pK_{ai}}}{10^{pH} + 10^{pK_{ai}}} - \sum_j Nj \frac{10^{pH}}{10^{pH} + 10^{pK_{aj}}}$$

where i represents positive charges from the polypeptide N-terminus and the side chains of arginine, lysine, and histidine residues; j represents negative charges from the polypeptide C-terminus and the side chains of aspartic acid, glutamic acid, cysteine, and tyrosine residues; and N represents the number of charges of a particular sign.

Data Acquisition. The ionic current through a single aerolysin channel was measured using an Axopatch 200B amplifier. Data were filtered at 10 kHz (100 μs) and acquired at 250 kHz intervals (4 μs) using the DigiData 1440A digitizer with Clampex software (Axon Instruments, Union City, CA, USA).

The data processing is based on statistical methods. The baseline corresponds to the noisy ionic current through the empty pore, defined by its mean value $\langle I_0 \rangle$ and its standard deviation (σ). We separated the current drops from the noise by imposing that a pulse height must be larger than a given threshold in order to be considered as significant. A first threshold, th1, was defined by $\langle I_0 \rangle - 2\sigma$ in order to avoid ~95% of the noise fluctuations.[60,82] This threshold, however, was insufficient to separate bone fide translocation events from bumping events. Hence we also applied a higher threshold, th2 = $\langle I_0 \rangle - 3\sigma$, in order to distinguish blockades due to bumping from translocation events. This second threshold was checked from the histogram of the electric current of the whole trace. We observed three distinct populations: the first one is associated with the fluctuating baseline current, the second one corresponds to bumping events, and the third one to translocation events.

The average duration of blockades is deduced from the distribution of blockade duration, τ_t. The two blockade time distributions of independent events are adjusted with two separate exponential functions, $y = A_1 \exp(-t/\tau_1)$ and $y = A_2 \exp(-t/\tau_2)$, and with a double exponential function, $y = A_1 \exp(-t/\tau_1) + A_2 \exp(-t/\tau_2)$. Each blockade duration is the average of these two characteristic times. All statistical analyses were performed using Igor Pro software (WaveMetrics Inc.).

Calculation of Hydrodynamic Properties. The expected diffusional properties of unfolded pertactin monomers and dimers were calculated using the structure-based hydrodynamic modeling program HYDROPRO.[55] Twelve putative structures of the unfolded state of our pertactin monomer construct were generated with the program RCG, developed by the Freed and Sosnick groups to model the unfolded states of proteins.[83] Side chains were added to all structures using the rotamer modeling program SCWRL4.0;[84] the resulting structures were visualized using VMD[85] and are shown in Figure S1e. The 12 structures of the pertactin monomer were then used to generate 144 putative models of the C-terminal-fused pertactin dimer by superimposing the side chain atoms of the final cysteine residues in all possible combinations of two copies of the monomer. Translational diffusion coefficients for the 12 monomer and the 144 dimer structures were computed with HYDROPRO using default settings and assuming solvent properties appropriate to a temperature of 298.15 K. The mean computed translational diffusion coefficient for the monomer is $2.81 \pm 0.32 \times 10^{-7}$ Å^2 ps^{-1} (min value = 2.44×10^{-7} Å^2 ps^{-1}; max value = 3.52×10^{-7} Å^2 ps^{-1}). The mean computed translational diffusion coefficient for the dimer is $(1.98 \pm 0.23) \times 10^{-7}$ Å^2 ps^{-1} (min value = 1.58×10^{-7} Å^2 ps^{-1}; max value = 2.90×10^{-7} Å^2 ps^{-1}).

Conflict of Interest: The authors declare no competing financial interest.

Acknowledgment. We thank Tobin Sosnick for helpful discussions, and Matteo Del Peraro for providing the aerolysin ribbon diagram figure. This project was supported by awards from the National Institutes of Health to P.L.C. (R01 GM097573) and P.L.C. and A.H.E. (U54 GM105816). E.B. was supported by a Notre Dame CBBI Graduate Fellowship (T32 GM075762). A.O. and J.P. thank the Agence Nationale de la Recherche (ANR 12-NANO-0012-03) and the Region Ile-de-France in the Framework of DIM Nano-K (No. 094251) for support.

Supporting Information Available: The Supporting Information is available free of charge on the ACS Publications website at DOI: 10.1021/acsnano.5b03053.

Supporting figure, corresponding to complementary results and experimental methods (PDF)

REFERENCES AND NOTES

1. Rapoport, T. A. Protein Translocation Across the Eukaryotic Endoplasmic Reticulum and Bacterial Plasma Membranes. *Nature* **2007**, *450*, 663–669.
2. Robson, A.; Collinson, I. The Structure of the Sec Complex and the Problem of Protein Translocation. *EMBO Rep.* **2006**, *7*, 1099–1103.
3. Schatz, G.; Dobberstein, B. Common Principles of Protein Translocation Across Membranes. *Science* **1996**, *271*, 1519–1526.
4. Matouschek, A.; Azem, A.; Ratliff, K.; Glick, B. S.; Schmid, K.; Schatz, G. Active Unfolding of Precursor Proteins During Mitochondrial Protein Import. *EMBO J.* **1997**, *16*, 6727–6736.
5. Neupert, W.; Brunner, M. The Protein Import Motor of Mitochondria. *Nat. Rev. Mol. Cell Biol.* **2002**, *3*, 555–565.
6. De Los Rios, P.; Ben-Zvi, A.; Slutsky, O.; Azem, A.; Goloubinoff, P. Hsp70 Chaperones Accelerate Protein Translocation and the Unfolding of Stable Protein Aggregates by Entropic Pulling. *Proc. Natl. Acad. Sci. U. S. A.* **2006**, *103*, 6166–6171.
7. Stefureac, R.; Long, Y.-T.; Kraatz, H.-B.; Howard, P.; Lee, J. S. Transport of Alpha-Helical Peptides through Alpha-Hemolysin and Aerolysin Pores. *Biochemistry* **2006**, *45*, 9172–9179.
8. Wang, H.-Y.; Ying, Y.-L.; Li, Y.; Kraatz, H.-B.; Long, Y.-T. Nanopore Analysis of β-Amyloid Peptide Aggregation Transition Induced by Small Molecules. *Anal. Chem.* **2011**, *83*, 1746–1752.
9. Sutherland, T. C.; Long, Y.-T.; Stefureac, R.-I.; Bediako-Amoa, I.; Kraatz, H.-B.; Lee, J. S. Structure of Peptides Investigated by Nanopore Analysis. *Nano Lett.* **2004**, *4*, 1273–1277.
10. Meng, H.; Detillieux, D.; Baran, C.; Krasniqi, B.; Christensen, C.; Madampage, C.; Stefureac, R. I.; Lee, J. S. Nanopore Analysis of Tethered Peptides. *J. Pept. Sci.* **2010**, *16*, 701–708.
11. Mereuta, L.; Roy, M.; Asandei, A.; Lee, J. K.; Park, Y.; Andricioaei, I.; Luchian, T. Slowing Down Single-Molecule Trafficking through a Protein Nanopore Reveals Intermediates for Peptide Translocation. *Sci. Rep.* **2014**, *4*, 3885.
12. Pastoriza-Gallego, M.; Rabah, L.; Gibrat, G.; Thiebot, B.; van der Goot, F. G.; Auvray, L.; Betton, J.-M.; Pelta, J. Dynamics of Unfolded Protein Transport through an Aerolysin Pore. *J. Am. Chem. Soc.* **2011**, *133*, 2923–2931.
13. Jetha, N. N.; Semenchenko, V.; Wishart, D. S.; Cashman, N. R.; Marziali, A. Nanopore Analysis of Wild-Type and Mutant Prion Protein (PrP(C)): Single Molecule Discrimination and PrP(C) Kinetics. *PLoS One* **2013**, *8*, e54982–e54982.
14. Mahendran, K. R.; Romero-Ruiz, M.; Schlösinger, A.; Winterhalter, M.; Nussberger, S. Protein Translocation through Tom40: Kinetics of Peptide Release. *Biophys. J.* **2012**, *102*, 39–47.
15. Mohammad, M. M.; Movileanu, L. Excursion of a Single Polypeptide Into a Protein Pore: Simple Physics, but Complicated Biology. *Eur. Biophys. J.* **2008**, *37*, 913–925.
16. Movileanu, L.; Schmittschmitt, J. P.; Scholtz, J. M.; Bayley, H. Interactions of Peptides with a Protein Pore. *Biophys. J.* **2005**, *89*, 1030–1045.
17. Madampage, C. A.; Andrievskaia, O.; Lee, J. S. Nanopore Detection of Antibody Prion Interactions. *Anal. Biochem.* **2010**, *396*, 36–41.

18. Oukhaled, G.; Mathe, J.; Biance, A. L.; Bacri, L.; Betton, J.-M.; Lairez, D.; Pelta, J.; Auvray, L. Unfolding of Proteins and Long Transient Conformations Detected by Single Nanopore Recording. *Phys. Rev. Lett.* **2007**, *98*, 158101.
19. Merstorf, C.; Cressiot, B.; Pastoriza-Gallego, M.; Oukhaled, A.; Betton, J.-M.; Auvray, L.; Pelta, J. Wild Type, Mutant Protein Unfolding and Phase Transition Detected by Single-Nanopore Recording. *ACS Chem. Biol.* **2012**, *7*, 652–658.
20. Payet, L.; Martinho, M.; Pastoriza-Gallego, M.; Betton, J.-M.; Auvray, L.; Pelta, J.; Mathé, J. Thermal Unfolding of Proteins Probed at the Single Molecule Level Using Nanopores. *Anal. Chem.* **2012**, *84*, 4071–4076.
21. Rodriguez-Larrea, D.; Bayley, H. Multistep Protein Unfolding During Nanopore Translocation. *Nat. Nanotechnol.* **2013**, *8*, 288–295.
22. Rodriguez-Larrea, D.; Bayley, H. Protein Co-Translocational Unfolding Depends on the Direction of Pulling. *Nat. Commun.* **2014**, *5*, 4841–4841.
23. Nivala, J.; Marks, D. B.; Akeson, M. Unfoldase-Mediated Protein Translocation through an A-Hemolysin Nanopore. *Nat. Biotechnol.* **2013**, *31*, 247–250.
24. Nivala, J.; Mulroney, L.; Li, G.; Schreiber, J.; Akeson, M. Discrimination Among Protein Variants Using an Unfoldase-Coupled Nanopore. *ACS Nano* **2014**, *8*, 12365–12375.
25. Stefureac, R.; Waldner, L.; Howard, P.; Lee, J. Nanopore Analysis of a Small 86-Residue Protein. *Small* **2008**, *4*, 59–63.
26. Baran, C.; Smith, G. S. T.; Bamm, V. V.; Harauz, G.; Lee, J. S. Divalent Cations Induce a Compaction of Intrinsically Disordered Myelin Basic Protein. *Biochem. Biophys. Res. Commun.* **2010**, *391*, 224–229.
27. Rosen, C. B.; Rodriguez-Larrea, D.; Bayley, H. Single-Molecule Site-Specific Detection of Protein Phosphorylation with a Nanopore. *Nat. Biotechnol.* **2014**, *32*, 179–181.
28. Degiacomi, M. T.; Iacovache, I.; Pernot, L.; Chami, M.; Kudryashev, M.; Stahlberg, H.; van der Goot, F. G.; Dal Peraro, M. Molecular Assembly of the Aerolysin Pore Reveals a Swirling Membrane-Insertion Mechanism. *Nat. Chem. Biol.* **2013**, *9*, 623–629.
29. Parker, M. W.; Buckley, J. T.; Postma, J. P.; Tucker, A. D.; Leonard, K.; Pattus, F.; Tsernoglou, D. Structure of the Aeromonas Toxin Proaerolysin in Its Water-Soluble and Membrane-Channel States. *Nature* **1994**, *367*, 292–295.
30. Zhai, Y.; Zhang, K.; Huo, Y.; Zhu, Y.; Zhou, Q.; Lu, J.; Black, I.; Pang, X.; Roszak, A. W.; Zhang, X.; et al. Autotransporter Passenger Domain Secretion Requires a Hydrophobic Cavity at the Extracellular Entrance of the β-Domain Pore. *Biochem. J.* **2011**, *435*, 577–587.
31. Barnard, T. J.; Dautin, N.; Lukacik, P.; Bernstein, H. D.; Buchanan, S. K. Autotransporter Structure Reveals Intra-Barrel Cleavage Followed by Conformational Changes. *Nat. Struct. Mol. Biol.* **2007**, *14*, 1214–1220.
32. Tajima, N.; Kawai, F.; Park, S.-Y.; Tame, J. R. H. A Novel Intein-Like Autoproteolytic Mechanism in Autotransporter Proteins. *J. Mol. Biol.* **2010**, *402*, 645–656.
33. Saurí, A.; ten Hagen-Jongman, C. M.; van Ulsen, P.; Luirink, J. Estimating the Size of the Active Translocation Pore of an Autotransporter. *J. Mol. Biol.* **2012**, *416*, 335–345.
34. Gawarzewski, I.; DiMaio, F.; Winterer, E.; Tschapek, B.; Smits, S. H. J.; Jose, J.; Schmitt, L. Crystal Structure of the Transport Unit of the Autotransporter Adhesin Involved in Diffuse Adherence From *Escherichia coli*. *J. Struct. Biol.* **2014**, *187*, 20–29.
35. Van den Berg, B. Crystal Structure of a Full-Length Autotransporter. *J. Mol. Biol.* **2010**, *396*, 627–633.
36. Oomen, C. J.; van Ulsen, P.; Van Gelder, P.; Feijen, M.; Tommassen, J.; Gros, P. Structure of the Translocator Domain of a Bacterial Autotransporter. *EMBO J.* **2004**, *23*, 1257–1266.
37. Noinaj, N.; Kuszak, A. J.; Gumbart, J. C.; Lukacik, P.; Chang, H.; Easley, N. C.; Lithgow, T.; Buchanan, S. K. Structural Insight Into the Biogenesis of β-Barrel Membrane Proteins. *Nature* **2013**, *501*, 385–390.
38. Gruss, F.; Zähringer, F.; Jakob, R. P.; Burmann, B. M.; Hiller, S.; Maier, T. The Structural Basis of Autotransporter Translocation by TamA. *Nat. Struct. Mol. Biol.* **2013**, *20*, 1318–1320.
39. Jong, W. S. P.; ten Hagen-Jongman, C. M.; den Blaauwen, T.; Slotboom, D. J.; Tame, J. R. H.; Wickström, D.; de Gier, J.-W.; Otto, B. R.; Luirink, J. Limited Tolerance Towards Folded Elements During Secretion of the Autotransporter Hbp. *Mol. Microbiol.* **2007**, *63*, 1524–1536.
40. Junker, M.; Besingi, R. N.; Clark, P. L. Vectorial Transport and Folding of an Autotransporter Virulence Protein During Outer Membrane Secretion. *Mol. Microbiol.* **2009**, *71*, 1323–1332.
41. Renn, J. P.; Junker, M.; Besingi, R. N.; Braselmann, E.; Clark, P. L. ATP-Independent Control of Autotransporter Virulence Protein Transport *via* the Folding Properties of the Secreted Protein. *Chem. Biol.* **2012**, *19*, 287–296.
42. Pastoriza-Gallego, M.; Breton, M.-F.; Discala, F.; Auvray, L.; Betton, J.-M.; Pelta, J. Evidence of Unfolded Protein Translocation through a Protein Nanopore. *ACS Nano* **2014**, *8*, 11350–11360.
43. Oukhaled, A.; Bacri, L.; Pastoriza-Gallego, M.; Betton, J.-M.; Pelta, J. Sensing Proteins through Nanopores: Fundamental to Applications. *ACS Chem. Biol.* **2012**, *7*, 1935–1949.
44. Cressiot, B.; Oukhaled, A.; Bacri, L.; Pelta, J. Focus on Protein Unfolding through Nanopores. *BioNanoScience* **2014**, *4*, 111–118.
45. Dautin, N.; Bernstein, H. D. Protein Secretion in Gram-Negative Bacteria *via* the Autotransporter Pathway. *Annu. Rev. Microbiol.* **2007**, *61*, 89–112.
46. Drobnak, I.; Braselmann, E.; Clark, P. L. Multiple Driving Forces Required for Efficient Secretion of Autotransporter Virulence Proteins. *J. Biol. Chem.* **2015**, *290*, 10104–10116.
47. Smith, A. M. A.; Guzmán, C. A. C.; Walker, M. J. M. The Virulence Factors of Bordetella pertussis: a Matter of Control. *FEMS Microbiol. Rev.* **2001**, *25*, 309–333.
48. Emsley, P.; Charles, I. G.; Fairweather, N. F.; Isaacs, N. W. Structure of Bordetella Pertussis Virulence Factor P.69 Pertactin. *Nature* **1996**, *381*, 90–92.
49. Henrickson, S. E.; Misakian, M.; Robertson, B.; Kasianowicz, J. J. Driven DNA Transport Into an Asymmetric Nanometer-Scale Pore. *Phys. Rev. Lett.* **2000**, *85*, 3057–3060.
50. Meller, A.; Branton, D. Single Molecule Measurements of DNA Transport through a Nanopore. *Electrophoresis* **2002**, *23*, 2583–2591.
51. Japrung, D.; Henricus, M.; Li, Q.; Maglia, G.; Bayley, H. Urea Facilitates the Translocation of Single-Stranded DNA and RNA through the A-Hemolysin Nanopore. *Biophys. J.* **2010**, *98*, 1856–1863.
52. Brun, L.; Pastoriza-Gallego, M.; Oukhaled, G.; Mathe, J.; Bacri, L.; Auvray, L.; Pelta, J. Dynamics of Polyelectrolyte Transport through a Protein Channel as a Function of Applied Voltage. *Phys. Rev. Lett.* **2008**, *100*, 158302.
53. Gibrat, G.; Pastoriza-Gallego, M.; Thiebot, B.; Breton, M.-F.; Auvray, L.; Pelta, J. Polyelectrolyte Entry and Transport through an Asymmetric Alpha-Hemolysin Channel. *J. Phys. Chem. B* **2008**, *112*, 14687–14691.
54. Oukhaled, G.; Bacri, L.; Mathe, J.; Pelta, J.; Auvray, L. Effect of Screening on the Transport of Polyelectrolytes through Nanopores. *Europhys. Lett.* **2008**, *82*, 48003.
55. Ortega, A.; Amoros, D.; Garcia de la Torre, J. Prediction of Hydrodynamic and Other Solution Properties of Rigid Proteins From Atomic- and Residue-Level Models. *Biophys. J.* **2011**, *101*, 892–898.
56. Muthukumar, M. *Polymer Translocation*; CRC Press: Boca Raton, FL, 2011; pp 9−11.
57. Mohammad, M. M.; Prakash, S.; Matouschek, A.; Movileanu, L. Controlling a Single Protein in a Nanopore through Electrostatic Traps. *J. Am. Chem. Soc.* **2008**, *130*, 4081–4088.
58. Pastoriza-Gallego, M.; Gibrat, G.; Thiebot, B.; Betton, J.-M.; Pelta, J. Polyelectrolyte and Unfolded Protein Pore Entrance Depends on the Pore Geometry. *Biochim. Biophys. Acta, Biomembr.* **2009**, *1788*, 1377–1386.
59. Muthukumar, M. Communication: Charge, Diffusion, and Mobility of Proteins through Nanopores. *J. Chem. Phys.* **2014**, *141*, 081104.
60. Kasianowicz, J. J.; Brandin, E.; Branton, D.; Deamer, D. W. Characterization of Individual Polynucleotide Molecules

Using a Membrane Channel. *Proc. Natl. Acad. Sci. U. S. A.* **1996**, *93*, 13770–13773.
61. Cressiot, B.; Oukhaled, A.; Patriarche, G.; Pastoriza-Gallego, M.; Betton, J.-M.; Auvray, L.; Muthukumar, M.; Bacri, L.; Pelta, J. Protein Transport through a Narrow Solid-State Nanopore at High Voltage: Experiments and Theory. *ACS Nano* **2012**, *6*, 6236–6243.
62. Wilmsen, H. U.; Pattus, F.; Buckley, J. T. Aerolysin, a Hemolysin From Aeromonas Hydrophila, Forms Voltage-Gated Channels in Planar Lipid Bilayers. *J. Membr. Biol.* **1990**, *115*, 71–81.
63. Lairez, D.; Pauthe, E.; Pelta, J. Refolding of a High Molecular Weight Protein: Salt Effect on Collapse. *Biophys. J.* **2003**, *84*, 3904–3916.
64. Flory, P. J. *Principles of Polymer Chemistry*; Cornell University Press: New York, 1953; pp 69−105.
65. Makarov, D. E. Computer Simulations and Theory of Protein Translocation. *Acc. Chem. Res.* **2009**, *42*, 281–289.
66. Muthukumar, M. Mechanism of DNA Transport through Pores. *Annu. Rev. Biophys. Biomol. Struct.* **2007**, *36*, 435–450.
67. de Gennes, P.-G. Flexible Polymers in Nanopores. In *Polymers in Confined Environments*; Granick, S., Binder, K., de Gennes, P. G., Giannelis, E., Grest, G., Hervet, H., Krishnamoorti, R., Léger, L., Manias, E., Raphael, E., Eds.; Advances in Polymer Science; Springer: Berlin, 1999; Vol. 138, pp 91−105.
68. Terentjev, E. M; Weitz, D. A. *The Oxford Handbook of Soft Condensed Matter*; Oxford University Press: New York, 2015; pp 399−410.
69. Vaitheeswaran, S.; Thirumalai, D. Entropy and Enthalpy of Interaction Between Amino Acid Side Chains in Nanopores. *J. Chem. Phys.* **2014**, *141*, 22D523.
70. Bezrukov, S. M.; Kasianowicz, J. J. The Charge State of an Ion Channel Controls Neutral Polymer Entry Into Its Pore. *Eur. Biophys. J.* **1997**, *26*, 471–476.
71. Breton, M.-F.; Discala, F.; Bacri, L.; Foster, D.; Pelta, J.; Oukhaled, A. Exploration of Neutral Versus Polyelectrolyte Behavior of Poly (Ethylene Glycol) S in Alkali Ion Solutions Using Single-Nanopore Recording. *J. Phys. Chem. Lett.* **2013**, *4*, 2202–2208.
72. Movileanu, L.; Cheley, S.; Bayley, H. Partitioning of Individual Flexible Polymers Into a Nanoscopic Protein Pore. *Biophys. J.* **2003**, *85*, 897–910.
73. Freedman, K. J.; Haq, S. R.; Edel, J. B.; Jemth, P.; Kim, M. J. Single Molecule Unfolding and Stretching of Protein Domains Inside a Solid-State Nanopore by Electric Field. *Sci. Rep.* **2013**, *3*, 1638.
74. Uplinger, J.; Thomas, B.; Rollings, R.; Fologea, D.; McNabb, D.; Li, J. K + , Na + , and Mg 2+ on DNA Translocation in Silicon Nitride Nanopores. *Electrophoresis* **2012**, *33*, 3448–3457.
75. Manning, G. S. Limiting Laws and Counterion Condensation in Polyelectrolyte Solutions I. Colligative Properties. *J. Chem. Phys.* **1969**, *51*, 924–933.
76. Daoud, M.; de Gennes, P. G. Statistics of Macromolecular Solutions Trapped in Small Pores. *J. Phys. (Paris)* **1977**, *38*, 85–93.
77. Junker, M.; Schuster, C. C.; McDonnell, A. V.; Sorg, K. A.; Finn, M. C.; Berger, B.; Clark, P. L. Pertactin Beta-Helix Folding Mechanism Suggests Common Themes for the Secretion and Folding of Autotransporter Proteins. *Proc. Natl. Acad. Sci. U. S. A.* **2006**, *103*, 4918–4923.
78. Montal, M.; Mueller, P. Formation of Bimolecular Membranes From Lipid Monolayers and a Study of Their Electrical Properties. *Proc. Natl. Acad. Sci. U. S. A.* **1972**, *69*, 3561–3566.
79. Moniatte, M.; vanderGoot, F. G.; Buckley, J. T.; Pattus, F.; vanDorsselaer, A. Characterisation of the Heptameric Pore-Forming Complex of the Aeromonas Toxin Aerolysin Using MALDI-TOF Mass Spectrometry. *FEBS Lett.* **1996**, *384*, 269–272.
80. Cabiaux, V.; Buckley, J. T.; Wattiez, R.; Ruysschaert, J. M.; Parker, M. W.; van der Goot, F. G. Conformational Changes in Aerolysin During the Transition From the Water-Soluble Protoxin to the Membrane Channel. *Biochemistry* **1997**, *36*, 15224–15232.
81. Tanford, C. The Interpretation of Hydrogen Ion Titration Curves of Proteins. *Adv. Protein. Chem.* **1962**, *17*, 69–165.
82. Reiner, J. E.; Kasianowicz, J. J.; Nablo, B. J.; Robertson, J. W. F. Theory for Polymer Analysis Using Nanopore-Based Single-Molecule Mass Spectrometry. *Proc. Natl. Acad. Sci. U. S. A.* **2010**, *107*, 12080–12085.
83. Jha, A. K.; Colubri, A.; Freed, K. F.; Sosnick, T. R. Statistical Coil Model of the Unfolded State: Resolving the Reconciliation Problem. *Proc. Natl. Acad. Sci. U. S. A.* **2005**, *102*, 13099–13104.
84. Krivov, G. G.; Shapovalov, M. V.; Dunbrack, R. L. J. Improved Prediction of Protein Side-Chain Conformations with SCWRL4. *Proteins: Struct., Funct., Genet.* **2009**, *77*, 778–795.
85. Humphrey, W.; Dalke, A.; Schulten, K. VMD: Visual Molecular Dynamics. *J. Mol. Graphics* **1996**, *14*, 33–38.